Patterns of Flexible Nanotubes Formed by Liquid-Ordered and Liquid-Disordered Membranes - Supporting Information

Yonggang Liu[†,‡], Jaime Agudo-Canalejo[†], Andrea Grafmüller[†], Rumiana Dimova[†] and Reinhard Lipowsky[†*]

[†] *Theory and Bio-Systems, Max Planck Institute of Colloids and Interfaces, Science Park Golm, 14424 Potsdam, Germany*
[‡] *State Key Laboratory of Polymer Physics and Chemistry, Changchun Institute of Applied Chemistry, Chinese Academy of Sciences, 130022 Changchun, China*

November 20, 2015

This Supporting Information contains the following items:

Supporting Sections:
Sect. S1: Critical tube length for VM-A and VM-B morphologies.
Sect. S2: Critical tube length for VM-C morphologies.
Sect. S3: Tube flexibility and persistence length.

Supporting Figures:
Fig. S1: Shapes of aqueous droplets for different vesicle morphologies.
Fig. S2: Vertical cross sections of the Ld and Lo vesicles in Fig. 2.
Fig. S3: Contact angles for VM-C morphologies.
Fig. S4: Adhesion of membrane nanotubes to the pd interface.
Fig. S5: Different tube shapes with the same membrane area and tube length.

Supporting Tables:
Table S1: Deflation path within the phase diagram of Fig. 2.
Table S2: Geometry of deflated Ld_j and Lo_j vesicles.
Table S3: Overlap of PEG and dextran chains along the deflation path.

Captions for the Movies Ld_j and Lo_j with $j = 1, 2, 4$.

References for Supporting Information

S1 Critical tube length for VM-A and VM-B morphologies

S1.1 Giant vesicle with necklace-like tube

Consider a giant vesicle with a spherical shape of radius R_0. The vesicle membrane has a large and negative spontaneous curvature m which favors highly curved membrane segments, in contrast to the small curvature $1/R_0$ of the initial vesicle. When the vesicle volume is reduced by osmotic deflation, the membrane can form an '$\mathcal{N}$-shape' consisting of a large spherical mother vesicle together with a necklace-like tube that protrudes into the vesicle interior. We have determined the $\mathcal{N}$-shapes of minimal bending energy as a function of reduced volume

$$v \equiv \frac{V}{V_0} \leq 1 \quad \text{with} \quad V_0 \equiv \tfrac{4\pi}{3} R_0^3 \tag{S1}$$

where $v = 1$ corresponds to the spherical mother vesicle without a necklace-like tube. The results of the numerical energy minimization, which are based on the shape functional in Eq. 3 of the main text, are displayed in Fig. 5.

The $\mathcal{N}$-shapes of minimal bending energy contain the shapes $L^{[N]}$ for which the necklace consists of N spherical beads with radius $R_{\rm ss} = 1/|m|$, see Fig. 5. Such a necklace-like tube has constant mean curvature $M = m$ and, thus, vanishing bending energy as follows from Eq. 3 of the main text. Furthermore, the mother vesicle has the radius

$$R_N = R_0 \sqrt{1 - \frac{N}{(|m|R_0)^2}} < R_0 \tag{S2}$$

as obtained from the conservation of membrane area which has the form

$$A_0 = 4\pi R_0^2 = 4\pi R_N^2 + N 4\pi |m|^{-2} . \tag{S3}$$

The necklace is anchored to the mother vesicle by an ideal membrane neck. The latter neck is formed as one approaches the limit shape $L^{\rm sto}$ from the branch of stomatocytes. [1] Likewise, the $L^{[N]}$-shapes with $N \geq 2$ also represent limit shapes which are obtained from necklace-like tubes with open necks, see Fig. 5. The $L^{[1]}$-shape is special because the necklace consists of a single spherical bead (or bud) which is obtained from the limit shape $L^{\rm sto}$ by increasing the bead radius from $R_{\rm ss} = 1/(2|m|)$ to $R_{\rm ss} = 1/|m|$. The $L^{[N]}$-shapes with $N \geq 2$ contain two types of ideal necks, the anchor neck between the mother vesicle and the first bead as well as the ss-ss necks between the small spheres of the necklace. Both types of membrane necks are stable provided $R_{\rm ss} \geq 1/|m|$ [2] which includes the limiting case $R_{\rm ss} = 1/|m|$ considered here.

The volume of the $L^{[N]}$-shapes is given by

$$V_N = \tfrac{4\pi}{3} R_N^3 - N \tfrac{4\pi}{3} R_{\rm ss}^3 = V_0 \left(\left[1 - \frac{N}{(|m|R_0)^2} \right]^{3/2} - \frac{N}{(|m|R_0)^3} \right) \tag{S4}$$

which decreases monotonically with increasing number N of the small beads. There-fore, the sequence of $L^{[N]}$-shapes provides a possible, low-energy pathway for osmotic deflation as depicted in Fig. 5 in the main text.

Because the bending energy of the necklace-like tube with $R_{ss} = 1/|m|$ vanishes, the bending energy of the $L^{[N]}$-shapes arises from the mother vesicle alone, $i.e.$,

$$\mathcal{E}_{be}\left(L^{[N]}\right) = 8\pi\kappa \ (1 - mR_N)^2 \tag{S5}$$

which is equivalent to

$$\mathcal{E}_{be}\left(L^{[N]}\right) = 8\pi\kappa \left[1 + |m|R_0\sqrt{1 - \frac{N}{(|m|R_0)^2}}\right]^2 . \tag{S6}$$

This energy also decreases monotonically with increasing bead number N, compare Fig. 5.

S1.2   Giant vesicle with cylindrical tube

We now transform the $L^{[N]}$-shapes as considered in the previous section into alter-native $C^{[N]}$-shapes for which the necklace-like tubes are replaced by cylindrical ones. For each value of N, we perform this transformation in such a way that *both the membrane area and the vesicle volume are conserved.*

The cylindrical tubes consist of cylinders that are closed by two spherical caps, where one of these end caps is connected to the mother vesicle by an ideal neck. The body of such a cylinder has length L_{cy}, radius $R_{cy} = 1/(2|m|)$, and mean curvature $M = m$ which implies that this membrane segment has vanishing bending energy. The radius of the mother vesicle is now denoted by R_{ls}. Because the $C^{[N]}$-shape is required to have the same membrane area as the $L^{[N]}$-shape, the length scales L_{cy} and R_{ls} are related *via*

$$R_{ls}^2 + \frac{1}{4|m|}L_{cy} + \frac{1}{4m^2} = R_N^2 + \frac{N}{m^2} . \tag{S7}$$

A second relation between these two scales is obtained from the requirement that the $C^{[N]}$-shape and the $L^{[N]}$-shape, which both include the mother vesicle, have the same volume which implies

$$R_{ls}^3 - \frac{3}{16m^2}L_{cy} - \frac{1}{8|m|^3} = R_N^3 - \frac{N}{|m|^3} . \tag{S8}$$

When we combine the two relations (S7) and (S8) to eliminate L_{cy}, we obtain the implicit equation

$$R_{ls}^3\left(1 + \frac{3}{4|m|R_{ls}}\right) = R_N^3\left(1 + \frac{3}{4|m|R_N}\right) - \frac{N + 1/4}{4|m|^3} \tag{S9}$$

3

for the mother vesicle radius R_{ls} of the $\mathcal{C}^{[N]}$-shape where R_N can be expressed in terms of R_0 *via* (S2). The implicit equation (S9) directly implies that $R_{\mathrm{ls}} < R_N$ for all positive values of N. Therefore, the $\mathcal{C}^{[N]}$-shape has a smaller mother vesicle and the membrane area stored in the cylinder exceeds the area stored in the N-necklace. We now define the parameter ϵ *via*

$$R_{\mathrm{ls}} = R_N \left(1 - \epsilon\right) \tag{S10}$$

and consider the limit of large $|m|R_0$, in which we obtain the asymptotic equality

$$\epsilon \approx \frac{N + 1/4}{12} \left(\frac{1}{|m|R_0}\right)^3 \quad \text{(large } |m|R_0) \tag{S11}$$

from the implicit equation (S9).

The bending energy of the $C^{[N]}$-shape is equal to

$$\mathcal{E}_{\mathrm{be}} \left(C^{[N]}\right) = 8\pi\kappa(1 - mR_{\mathrm{ls}})^2 + 2\pi\kappa \tag{S12}$$

where the first and the second term represents the energy contributions from the mother vesicle and from the two end caps of the cylinder, respectively.

S1.3   Critical tube length for necklace-cylinder transformation

We now compare the bending energy (S12) of the $C^{[N]}$-shape with the bending energy (S5) of the $L^{[N]}$-shape. The mother vesicle of the $C^{[N]}$-shape has the bending energy $8\pi\kappa(1 - mR_{\mathrm{ls}})^2$ which is smaller than the bending energy $8\pi\kappa \left(1 - mR_N\right)^2$ of the $L^{[N]}$-shape because $R_{\mathrm{ls}} < R_N$ and $|m|R_{\mathrm{ls}} \gg 1$. However, the capped cylinder has the bending energy $2\pi\kappa$ whereas the necklace has vanishing bending energy. Therefore, when we transform the $L^{[N]}$-shape into the $C^{[N]}$-shape, we reduce the bending energy of the mother vesicle but increase the bending energy of the tube.

We now define the reduced difference

$$\Delta \equiv \frac{\mathcal{E}_{\mathrm{be}} \left(C^{[N]}\right) - \mathcal{E}_{\mathrm{be}} \left(L^{[N]}\right)}{8\pi\kappa} \tag{S13}$$

between the bending energies of the $C^{[N]}$- and the $L^{[N]}$-shape, which has the form

$$\Delta = (1 + |m|R_{\mathrm{ls}})^2 + \tfrac{1}{4} - (1 + |m|R_N)^2 \tag{S14}$$

or

$$\Delta = |m|(R_{\mathrm{ls}} - R_N) \left[2 + |m|(R_{\mathrm{ls}} + R_N)\right] + \tfrac{1}{4} \tag{S15}$$

Replacing R_{ls} by $R_N(1 - \epsilon)$, the latter relation becomes

$$\Delta = -\epsilon|m|R_N \left[2 + 2|m|R_N - \epsilon|m|R_N\right] + \tfrac{1}{4} . \tag{S16}$$

The $L^{[N]}$-shape and the $C^{[N]}$-shape are energetically favored for $\Delta > 0$ and $\Delta < 0$, respectively. The critical bead number N^* and the critical tube length

$$L_{\mathrm{tu}}^* = N^* 2R_{\mathrm{ss}} = N^* 2/|m| \tag{S17}$$

then follow from $\Delta = 0$.

In the limit of large $|m|R_0$ and small $\epsilon \sim (|m|R_0)^{-3}$, see (S11), we obtain the asymptotic equality

$$\Delta \approx -\frac{N + 1/4}{6|m|R_0} + \frac{1}{4} \tag{S18}$$

which implies the critical tube length

$$L_{\mathrm{tu}}^* = N^* 2/|m| \approx 3R_0 \,. \tag{S19}$$

It is interesting to note that exactly the same relation for the critical tube length is obtained if one replaces the bending energy contribution from the mother vesicle by the volume work performed on the tube by the pressure difference ΔP which behaves as $\Delta P \approx 4\kappa m^2/R_{\mathrm{ls}}$ for large $|m|R_{\mathrm{ls}}$ and acts to compress the necklace-like tube which has a larger volume than the cylindrical one. [3]

S1.4   Critical tube lengths for mother vesicle with many tubes

So far, we have explicitly discussed a mother vesicle with a single tube. However, the above considerations can be easily extended to a mother vesicle with several tubes. Indeed, all we have to do is to select one of the tubes and to redefine the membrane area and the membrane volume in an appropriate manner. Thus, let us label the selected tube by the index s and the remaining tubes by the index $r = 1, 2, \ldots$. The selected tube has the area A_s, the remaining tubes have the areas A_r. The redefined membrane area $\hat{A}_0$ is then given by

$$\hat{A}_0 \equiv A_0 - \sum_r A_r \equiv A_{\mathrm{mv}} + A_s \tag{S20}$$

with the area A_{mv} of the redefined mother vesicle. If we envisage to inflate this mother vesicle to retract the selected tube without changing the remaining tubes, we obtain a spherical vesicle with radius $\hat{R}_0 = [\hat{A}_0/(4\pi)]^{1/2}$ and volume $\hat{V}_0 = \frac{4\pi}{3}\hat{R}_0^3$.

Now, we have to replace the quantities R_0, V_0, and A_0 in Eqs. S1 - S3 by $\hat{R}_0, \hat{V}_0$, and $\hat{A}_0$ and to repeat the whole calculation with the hatted variables. In this way, we study the growth of the selected tube while all the other tubes remain unchanged. As a result, we obtain the critical length $\hat{L}_{\mathrm{tu}}^* \approx 3\hat{R}_0$ for the selected tube. Because the redefined vesicle radius $\hat{R}_0$ is smaller than R_0, the critical length $\hat{L}_{\mathrm{tu}}^*$ is smaller than L_{tu}^* for a vesicle with a single tube. This difference can, however, be neglected for the VM-A and VM-B morphologies studied here. Indeed, after the first two deflation steps, the total area of all membrane tubes, $A = A_s + \sum_r A_r$, satisfies $A \leq 0.1A_0$, see Fig. 3a in the main text, which implies that $\hat{A}_0 > 0.9A_0$ and $\hat{R}_0 > 0.948R_0$

irrespective of which individual tube we select. Therefore, the critical tube length $\hat{L}_{\mathrm{tu}}^*$ of any selected tube lies within the interval $2.84\,R_0 < \hat{L}_{\mathrm{tu}}^* \leq 3R_0$ and is always much larger than the individual tube lengths observed for the VM-A and VM-B morphologies.

When a necklace-like tube with length L_{tu}^* is transformed into a cylindrical tube of equal area A_{tu}^*, the tube length becomes twice as large. Therefore, in equilibrium, necklace-like tubes should have a length up to L_{tu}^* whereas cylindrical tubes should have a length exceeding $2L_{\mathrm{tu}}^*$. As a consequence, the length distribution of the tubes is predicted to exhibit a gap defined by the interval $L_{\mathrm{tu}}^* < L_{\mathrm{tu}} < 2L_{\mathrm{tu}}^*$.

S2 Critical tube length for VM-C morphologies

For the VM-C morphologies, the vesicle membrane is partially wetted by the two aqueous phases and the pe membrane segment separating the PEG-rich from the external phase forms the intrinsic contact angle θ_{in} with the pd interface. For the lipid-polymer systems studied here, all intrinsic contact angles were smaller than $90°$ (Fig. 8c in the main text).

Because of partial wetting, a membrane tube can lower its free energy by adhering to the pd interface. Furthermore, the large separation of length scales between the weakly curved pd interfaces and the strongly curved membrane tubes implies that we can ignore the interfacial curvature and consider the adhesion of the tubes to planar interfaces. In order to obtain explicit expressions for the corresponding adhesion free energies, we also ignore possible deformations of the tube shapes by the adhesion.

S2.1 Adhesion free energy of necklace-like tube

First, consider a necklace-like tube consisting of N spherical beads with radius $R_{\mathrm{ss}} = 1/|m|$ as in Fig. S4a. A single bead will immerse into the dextran-rich phase until the angle between the pd interface and the pe segment of the bead membrane is equal to the intrinsic contact angle θ_{in}. In the following, we will first consider an arbitrary contact angle θ and then require that the adhesion free energy attains its lowest value when this contact angle is equal to the intrinsic contact angle θ_{in}.

When the tube membrane forms the contact angle θ with the pd interface, the total surface area A_{nl} of the necklace-like tube is partitioned into two segments according to

$$A_{\mathrm{nl}} = N\,4\pi R_{\mathrm{ss}}^2 = N4\pi|m|^{-2} = A_{\mathrm{mp}} + A_{\mathrm{md}} \tag{S21}$$

with the contact area

$$A_{\mathrm{mp}} = N\,2\pi R_{\mathrm{ss}}^2(1 + \cos\theta) = N\,2\pi|m|^{-2}(1 + \cos\theta) \tag{S22}$$

6

between the inner leaflet of the membrane and the PEG-rich phase and and the contact area

$$A_{\mathrm{md}} = N \, 2\pi R_{\mathrm{ss}}^2 (1 - \cos\theta) = N \, 2\pi |m|^{-2} (1 - \cos\theta) \tag{S23}$$

between the inner leaflet of the membrane and the dextran-rich phase. At the same time, the area A_{pd} of the pd interface is reduced by

$$\Delta A_{\mathrm{pd}} = N \, \pi (R_{\mathrm{ss}} \sin\theta)^2 = N \, \pi |m|^{-2} \sin^2\theta \tag{S24}$$

The interfacial free energy of the pd interface and the free, non-adhering necklace fully immersed in the PEG-rich phase has the form

$$\mathcal{F}_{\mathrm{nl,fr}} = \Sigma_{\mathrm{pd}} \, A_{\mathrm{pd}} + \Sigma_{\mathrm{mp}} \, A_{\mathrm{nl}} \tag{S25}$$

with the interfacial tension Σ_{mp} of the interface between the inner leaflet of the membrane and the PEG-rich phase. Likewise, the interfacial free energy of the necklace adhering to the pd interface is given by

$$\mathcal{F}_{\mathrm{nl,ad}} = \Sigma_{\mathrm{pd}} \, (A_{\mathrm{pd}} - \Delta A_{\mathrm{pd}}) + \Sigma_{\mathrm{mp}} \, (A_{\mathrm{nl}} - A_{\mathrm{md}}) + \Sigma_{\mathrm{md}} \, A_{\mathrm{md}} \tag{S26}$$

with the interfacial tension Σ_{md} between the inner leaflet of the membrane and the dextran-rich phase. The adhesion free energy of the necklace-like tube is then given by

$$\mathcal{F}_{\mathrm{nl}} \equiv \mathcal{F}_{\mathrm{nl,ad}} - \mathcal{F}_{\mathrm{nl,fr}} = (\Sigma_{\mathrm{md}} - \Sigma_{\mathrm{mp}}) \, A_{\mathrm{md}} - \Sigma_{\mathrm{pd}} \, \Delta A_{\mathrm{pd}} \tag{S27}$$

or

$$\mathcal{F}_{\mathrm{nl}} = A_{\mathrm{nl}} \left[\tfrac{1}{2} (\Sigma_{\mathrm{md}} - \Sigma_{\mathrm{mp}})(1 - \cos\theta) - \tfrac{1}{4} \Sigma_{\mathrm{pd}} \sin^2\theta \right] . \tag{S28}$$

We now require that this free energy attains its equilibrium value when the contact angle θ becomes equal to the intrinsic contact angle θ_{in} corresponding to $\partial \mathcal{F}_{\mathrm{nl}}/\partial\theta = 0$ for $\theta = \theta_{\mathrm{in}}$. This requirement leads to

$$\Sigma_{\mathrm{md}} - \Sigma_{\mathrm{mp}} = \Sigma_{\mathrm{pd}} \, \cos\theta_{\mathrm{in}} \tag{S29}$$

and to the equilibrium value

$$\mathcal{F}_{\mathrm{nl}}^{\mathrm{eq}} = A_{\mathrm{nl}} \, \Sigma_{\mathrm{pd}} \, g_{\mathrm{nl}}(\theta_{\mathrm{in}}) \tag{S30}$$

for the adhesion free energy of the necklace-like tube with the angle-dependent function

$$g_{\mathrm{nl}}(\theta) \equiv \tfrac{1}{2} \, \cos\theta(1 - \cos\theta) - \tfrac{1}{4} \, \sin^2\theta = -\tfrac{1}{4} \, (1 - \cos\theta)^2 . \tag{S31}$$

The second expression for $g_{\mathrm{nl}}(\theta)$ implies that the adhesion free energy $\mathcal{F}_{\mathrm{nl}}^{\mathrm{eq}}$ is negative for nonzero values of the intrinsic contact angle θ_{in}, which shows explicitly that the adhering tube is energetically favored compared to the free tube immersed in the PEG-rich phase. Furthermore, the adhesion free energy density $\mathcal{F}_{\mathrm{nl}}^{\mathrm{eq}}/A_{\mathrm{nl}}$ as obtained from (S30) depends only on two material parameters, the interfacial tension Σ_{pd} of the pd interface and the intrinsic contact angle θ_{in}, both of which can be determined experimentally, see Fig. 3b and Fig. 8c in the main text.

7

S2.2 Adhesion free energy of cylindrical tube

Next, consider a cylindrical tube with two spherical end caps as in Fig. S4b. The body of the cylinder has length L_{cy} and radius $R_{cy} = 1/(2|m|)$; the spherical end caps have the same radius as the cylinder. These two membrane segments have the areas

$$A_{cy}^{bod} = 2\pi R_{cy} L_{cy} = \frac{\pi}{|m|} L_{cy} \quad \text{and} \quad A_{cy}^{cap} = 4\pi R_{cy}^2 = \frac{\pi}{m^2} . \tag{S32}$$

When the tube membrane forms the contact angle θ with the pd interface, the tube area A_{cy} is partitioned according to

$$A_{cy} = A_{cy}^{bod} + A_{cy}^{cap} = A_{mp} + A_{md} \tag{S33}$$

with the contact areas

$$A_{mp} = 2(\pi - \theta)R_{cy} L_{cy} + 2\pi R_{cy}^2 (1 + \cos\theta) \tag{S34}$$

and

$$A_{md} = 2\theta R_{cy} L_{cy} + 2\pi R_{cy}^2 (1 - \cos\theta) . \tag{S35}$$

At the same time, the area A_{pd} of the pd interface is reduced by

$$\Delta A_{pd} = 2R_{cy} L_{cy} \sin\theta + \pi R_{cy}^2 \sin^2\theta . \tag{S36}$$

The interfacial free energies $\mathcal{F}_{cy,fr}$ and $\mathcal{F}_{cy,ad}$ have the same general form as in (S25) and (S26). It then follows that the adhesion free energy of the cylindrical tube is given by

$$\mathcal{F}_{cy} = A_{cy}^{bod} G_{cy}^{bod} + A_{cy}^{cap} G_{cy}^{cap} \tag{S37}$$

with the body contribution

$$G_{cy}^{bod} \equiv (\Sigma_{md} - \Sigma_{mp})\frac{\theta}{\pi} - \Sigma_{pd}\frac{\sin\theta}{\pi} \tag{S38}$$

and the cap contribution

$$G_{cy}^{cap} \equiv (\Sigma_{md} - \Sigma_{mp})\tfrac{1}{2}(1 - \cos\theta) - \Sigma_{pd}\tfrac{1}{4}\sin^2\theta . \tag{S39}$$

The equilibrium value of the contact angle θ is again imposed by the condition $\partial \mathcal{F}_{cy}/\partial\theta = 0$ for $\theta = \theta_{in}$ which leads to the same relation $\Sigma_{md} - \Sigma_{mp} = \Sigma_{pd} \cos\theta_{in}$ as in (S29). As a consequence, the adhesion free energy of the capped cylindrical tube has the equilibrium form

$$\mathcal{F}_{cy}^{eq} = \Sigma_{pd} A_{cy}^{bod} g_{cy}(\theta_{in}) + \Sigma_{pd} A_{cy}^{cap} g_{nl}(\theta_{in}) \tag{S40}$$

with the function

$$g_{cy}(\theta) \equiv \frac{\theta}{\pi}\cos\theta - \frac{\sin\theta}{\pi} \tag{S41}$$

and the function $g_{nl}(\theta)$ as defined in (S31).

S2.3 Critical area and critical length of adhering tubes

We now compare an adhering necklace-like tube with an adhering cylindrical tube of the same tube area A_{tu} which then satisfies

$$A_{\text{tu}} = A_{\text{cy}} = A_{\text{nl}} \,. \tag{S42}$$

The bending energy of the necklace-like tube vanishes whereas the capped cylinder has the bending energy $2\pi\kappa$ arising from the spherical end caps as in (S12). Therefore, we have to consider the free energy difference

$$\Delta\mathcal{F} = \mathcal{F}_{\text{cy}}^{\text{eq}} + 2\pi\kappa - \mathcal{F}_{\text{nl}}^{\text{eq}} \tag{S43}$$

which can be rewritten in the form

$$\Delta\mathcal{F} = 2\pi\kappa - \Sigma_{\text{pd}} A_{\text{tu}} \left[1 - \frac{\pi}{m^2 A_{\text{tu}}}\right] g(\theta_{\text{in}}) \tag{S44}$$

with the function

$$g(\theta) \equiv g_{\text{nl}}(\theta) - g_{\text{cy}}(\theta) = \tfrac{1}{\pi}\left(\sin\theta - \theta\cos\theta\right) - \tfrac{1}{4}\left(1 - \cos\theta\right)^2 . \tag{S45}$$

As shown in Fig. S4c, the function $g(\theta)$ is positive for $0 < \theta < \pi$. Therefore, the shape of the adhering tube is determined by the competition between the bending energy $2\pi\kappa$ of the spherical caps, which favors necklace-like tubes, and the adhesion free energy, which favors cylindrical tubes. The spherical cap energy is independent of the tube area whereas the adhesion free energy is proportional to this area. As a consequence, short adhering tubes are necklace-like whereas long adhering tubes are cylindrical. These two regimes are separated by the critical tube area

$$A_{\text{tu}}^* = \frac{2\pi\kappa}{\Sigma_{\text{pd}}\, g(\theta_{\text{in}})} + \frac{\pi}{m^2} \tag{S46}$$

as follows from $\Delta\mathcal{F} = 0$. The first term directly reflects the interplay between the membrane's bending rigidity κ, the interfacial tension Σ_{pd}, and the intrinsic contact angle θ_{in} for partial wetting. The second term on the right hand side of (S46) represents a correction term arising from the spherical end caps.

In Fig. S4d, we compare the free energies of single necklace-like and cylindrical tubes as a function of tube area A_{tu} for the Ld_4 and the Lo_4 vesicles. The critical tube area is about $4.4\,\mu\text{m}^2$ for the Ld_4 vesicle and about $80.7\,\mu\text{m}^2$ for the Lo_4 vesicle.

From an experimental point, it is easier to measure the length of individual tubes rather than their area. The critical length $L_{\text{ad}}^* = N_{\text{ad}}^* 2/|m|$ of the necklace-like tube with the critical bead number N_{ad}^* is given by

$$L_{\text{ad}}^* = A_{\text{tu}}^* \frac{|m|}{2\pi} = \frac{\kappa|m|}{\Sigma_{\text{pd}}\, g(\theta_{\text{in}})} + \frac{1}{2|m|} \,. \tag{S47}$$

When a necklace-like tube with length L_{ad}^* is transformed into a cylindrical tube of equal area A_{tu}^*, the tube length becomes twice as large. Therefore, in equilibrium,

9

necklace-like tubes should have a length up to L_{ad}^* whereas cylindrical tubes should have a length exceeding $2L_{\mathrm{ad}}^*$. For the example displayed in Fig. S4d corresponding to the fourth deflation step, the critical tube length L_{ad}^* is $5.6\,\mu$m for the Ld_4 vesicle and $21.4\,\mu$m for the Lo_4 vesicle.

S3   Tube flexibility and persistence length

The flexibility of membrane nanotubes can be characterized by the persistence length for tube bending. This length scale governs the exponential decay of the two-point correlation function between unit tangent vectors along the tube, in close analogy to semiflexible polymers [4, 5]. A cylindrical tube of radius R_{cy} has the persistence length [6, 7]

$$\xi_p = 2\pi\kappa R_{\mathrm{cy}}/(k_{\mathrm{B}}T)\,. \tag{S48}$$

For $R_{\mathrm{cy}} = 1/(2|m|)$ corresponding to the state of lowest bending energy, this expression becomes

$$\xi_p = \frac{\pi\kappa}{|m|k_{\mathrm{B}}T}\,. \tag{S49}$$

Using the overall partitioning of the membrane area with total tube area A and total tube length L, a cylindrical tube has the spontaneous curvature $|m| = \pi L/A$ which implies the persistence length

$$\xi_p = \frac{\kappa}{k_{\mathrm{B}}T}\frac{A}{L} \quad \text{(cylindrical tube)}\,. \tag{S50}$$

The persistence length of the necklace-like tube, on the other hand, is comparable to the diameter $2R_{\mathrm{ss}} = 2/|m|$ of the small spheres which implies

$$\xi_p \simeq 2R_{\mathrm{ss}} = \frac{1}{\pi}\frac{A}{L} \quad \text{(necklace-like tube)}\,. \tag{S51}$$

For the Ld membrane studied here, the bending rigidity $\kappa_{\mathrm{Ld}} = 0.82 \times 10^{-19}\,$J and $\kappa_{\mathrm{Ld}}/(k_{\mathrm{B}}T) = 20$ at room temperature ($25°$C). For the Ld_1 vesicle, we obtained the total tube area $A = 473\,\mu$m^2 and the total tube length $L = 600\,\mu$m. If the tubes were cylindrical, we would obtain the spontaneous curvature $|m| = 1/(0.251\,\mu$m$)$ and the persistence length $\xi_p = 15.4\,\mu$m. If the tubes were necklace-like, we would obtain the spontaneous curvature $|m| = 1/(0.125\,\mu$m$)$ and the persistence length $\xi_p \simeq 0.25\,\mu$m. Inspection of the Movies Ld_1 and Ld_2 reveals that the thermal fluctuations of the tubes lead to hairpin-like conformations with curvature radii of the order of $2\,\mu$m which implies a persistence length below $2\,\mu$m. Such an upper bound for the persistence length is consistent with a necklace-like but not with a cylindrical tube morphology.
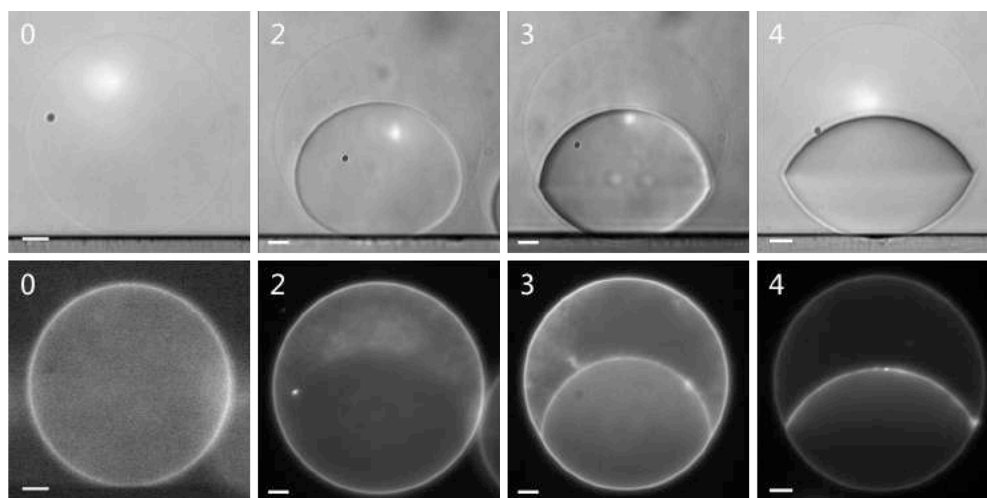
Figure S1: **Shapes of aqueous droplets for different vesicle morphologies:** The images correspond to Ld_j vesicles after the jth deflation step with $j = 0, 2, 3$, and 4 as observed by differential interference contrast (DIC) microscopy (top row) and fluorescence microscopy (bottom row). The two images with the same j-value display the same vesicle. The white scale bar is $10\,\mu$m in all panels. The images were obtained by a horizontally aligned inverted microscope (Axiovert 135, Zeiss) equipped with a 40x long distance objective and a mono-color camera.
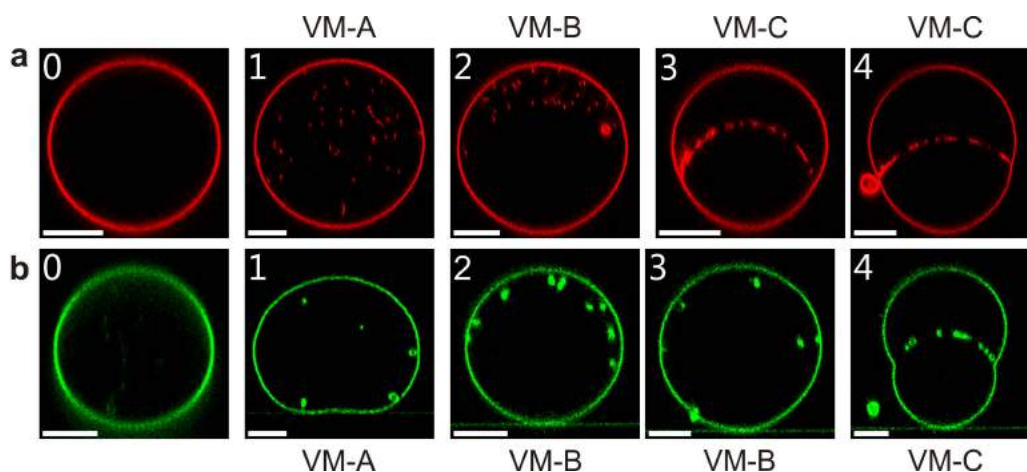

Figure S2: **Vertical cross sections of the Ld and Lo vesicles in Fig. 2:** **(a)** Confocal xz-scans of the Ld_j vesicles in Fig. 2c; and **(b)** Confocal xz-scans of the Lo_j vesicles in Fig. 2d. The three vesicle morphologies VM-A, VM-B, and VM-C are explained in Fig. 1.
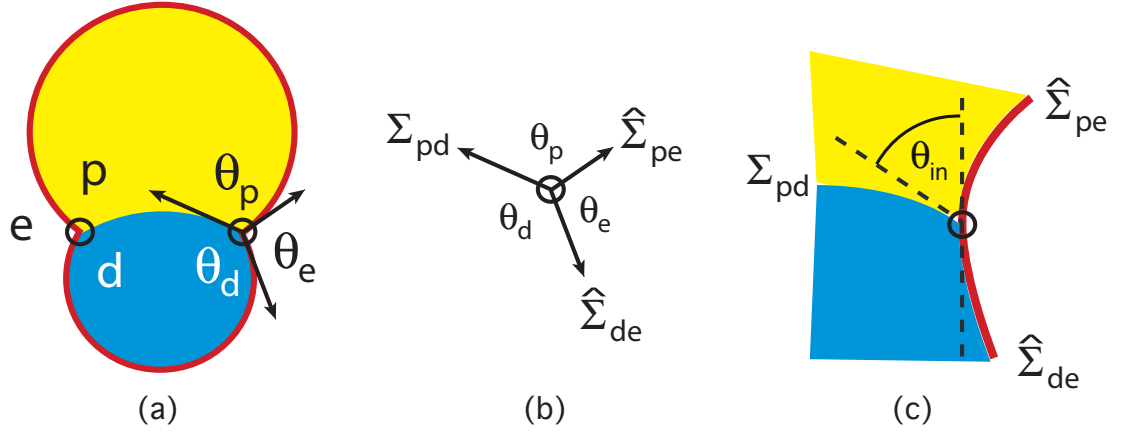
11

Figure S3: **Contact angles for the VM-C morphology:** The latter morphology involves one droplet of the PEG-rich phase p (yellow) and one droplet of the dextran-rich phase d (blue), both embedded in the exterior phase e (white): **(a)** The pd interface meets the membrane (red) along the contact line (two black circles). The latter line divides the membrane up into two segments, the pe segment between the PEG-rich droplet and the exterior phase as well as the de segment between the dextran-rich droplet and the exterior phase. When viewed with optical resolution, the membrane exhibits a kink at the contact line which defines the effective contact angles $\theta_{\mathrm{p}}, \theta_{\mathrm{d}}$, and θ_{e}; **(b)** The three arrows represent the interfacial tension Σ_{pd} as well as the two membrane tensions $\hat{\Sigma}_{\mathrm{pe}}$ and $\hat{\Sigma}_{\mathrm{de}}$ within the pe and de segments of the membrane. Mechanical equilibrium implies that the three tension vectors add up to zero; and **(c)** Enlarged view of the smoothly curved membrane (red) close to the contact line (black circle). The vertical broken line represents the common tangent plane of the two membrane segments. The angle between this common tangent plane and the plane tangential to the pd interface provides the intrinsic contact angle θ_{in}. [8] The membrane nanotubes have been omitted here in order to focus on the shape of the mother vesicle.
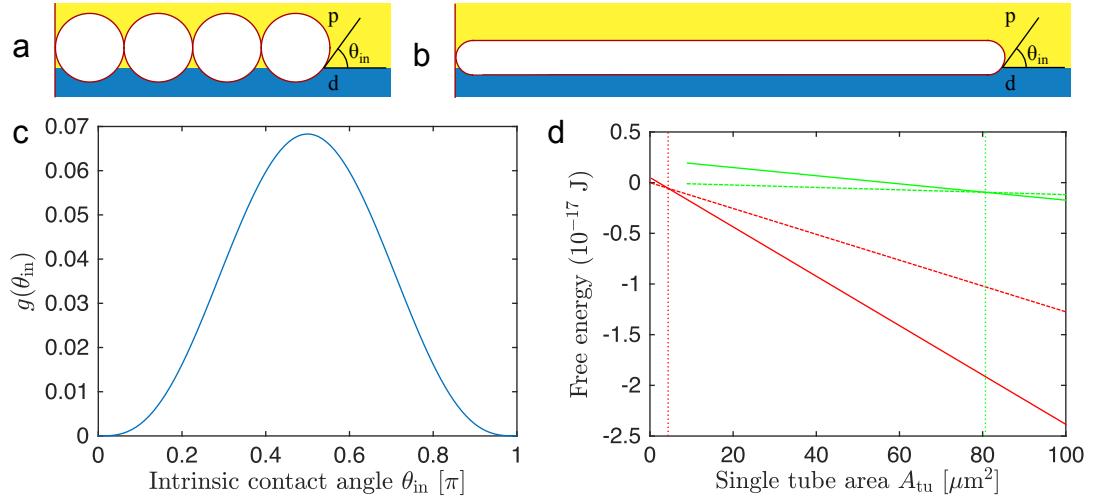
12

Figure S4: **Adhesion of membrane nanotubes to the pd interface (VM-C morphology): (a)** Necklace-like tube with four spherical beads and **(b)** Cylindrical tube with the same membrane area. Both tubes adhere to the pd interface which separates the PEG-rich phase p (yellow) from the dextran-rich phase d (blue) and forms the intrinsic contact angle θ_{in} with the tube membranes; **(c)** Functional dependence of the dimensionless free energy difference g on the intrinsic contact angle θ_{in} as given by equation (S45); and **(d)** Free energies of single necklace-like (dashed) and cylindrical (solid) tube protruding into the Ld_4 (red) and Lo_4 (green) vesicle as a function of tube area A_{tu} with $A_{tu} \geq 8\pi/m^2$ where the latter area corresponds to the 2-bead necklace $L^{[2]}$. The dashed and solid lines cross at the critical tube area A_{tu}^* which is equal to $4.4\,\mu m^2$ for the Ld_4 vesicle and to $80.7\,\mu m^2$ for the Lo_4 vesicle. The corresponding critical tube lengths are given by $L_{tu}^* = 5.6\,\mu m$ for the Ld_4 and by $L_{tu}^* = 21.4\,\mu m$ for the Lo_4 vesicle. The free energy of the necklace-like tubes is given by $\mathcal{F}_{nl}^{eq}$ as in equation (S30); the free energy of the cylindrical tubes is equal to $\mathcal{F}_{cy}^{eq} + 2\pi\kappa$ with $\mathcal{F}_{cy}^{eq}$ as in equation (S40).
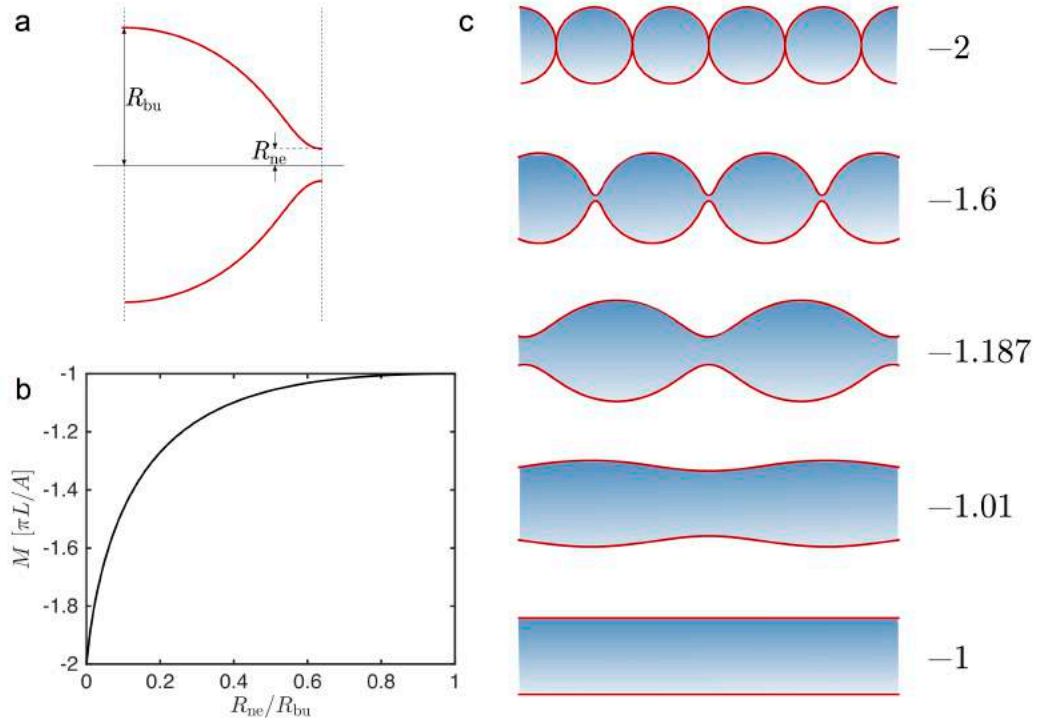
Figure S5: **Different tube shapes with the same membrane area and tube length:**
(a) Each unit cell of an unduloid is characterized by its neck radius R_{ne} and its bulge radius
R_{bu}. The necklace-like tube corresponds to the ratio $R_{\mathrm{ne}}/R_{\mathrm{bu}} = 0$, the cylindrical tube to
$R_{\mathrm{ne}}/R_{\mathrm{bu}} = 1$; **(b)** For given membrane area A and tube length L, the mean curvature M
increases monotonically from $M = -2\pi L/A$ for the necklace-like tube to $M = -\pi L/A$ for
the cylindrical tube; and **(c)** Three examples of unduloids for fixed A and L that interpolate
between the necklace-like and the cylindrical tube with mean curvature M in units of $\pi L/A$
(right column). As we transform the sphere-necklace into the cylinder, the neck radius
R_{ne} of the intermediate unduloid increases monotonically whereas the bulge radius R_{bu}
first increases and then decreases again. The latter radius has the value $A/(2\pi L)$ both for
the cylindrical tube and for the sphere-necklace and attains its maximum at $M = m = -1.187\pi L/A$ with $\max(R_{\mathrm{bu}}) = 0.662A/\pi L$.

14

Table S1: **Deflation path within the phase diagram of Fig. 2:** The deflation path in Fig. 2a,b consists of seven deflation steps which lead to seven compositions of the aqueous polymer solution within the vesicle, labeled from $j = 1$ to $j = 7$. The initial compositions in the exterior and interior solution are denoted by 0e and 0. The columns 2 - 7 display the following quantities: Dextran weight fraction w_d, PEG weight fraction w_p, total polymer mass density c_j of the interior solution, as well as concentration ratio c_j/c_0, osmolarity ratio P_e/P_0 between the exterior and the initial osmolarities, P_e and P_0. The exterior osmolarity P_e is increased by exchanging the external medium by a hypertonic solution with constant $w_d = w_p = 0.0327$ and an increasing weight fraction of sucrose. For $j \geq 0$, the weight fractions w_d and w_p represent the weight fractions of all dextran and all PEG molecules within the interior solution, irrespective of whether this solution is uniform or phase separated, and are characterized by the constant ratio $w_d/w_p = 1.25$. For comparison, the quantities at the critical point (cr) are also included. 'APS' stands for 'aqueous phase separation' in the vesicle interior. The last two rows describe the observed vesicle morphologies of the liquid-disordered (Ld) and liquid-ordered (Lo) membranes. The VM-B and VM-C morphologies correspond to phase separation with complete and partial wetting, respectively, of the membranes by the PEG-rich phase.

comp. j	w_d	w_p	c_j [g/cm^3]	c_j/c_0	P_e/P_0	APS	Ld morph.	Lo morph.
0e	0.0327	0.0327	0.0664		1.000	no		
0	0.0390	0.0312	0.0714	1.000	1.000	no		
1	0.0436	0.0349	0.0800	1.120	1.254	no	VM-A	VM-A
cr	0.0451	0.0361	0.0829	1.161	1.350	no		
2	0.0456	0.0365	0.0838	1.174	1.382	yes	VM-B	VM-B
3	0.0475	0.0380	0.0875	1.224	1.511	yes	VM-C	VM-B
4	0.0494	0.0395	0.0909	1.273	1.642	yes	VM-C	VM-C
5	0.0511	0.0408	0.0941	1.317	1.769	yes	VM-C	VM-C
6	0.0527	0.0422	0.0972	1.361	1.901	yes	VM-C	VM-C
7	0.0543	0.0434	0.1002	1.402	2.032	yes	VM-C	VM-C

Table S2: **Geometry of deflated Ld_j and Lo_j vesicles:** The first four rows give the lipid phase, the deflation step number (or polymer composition) j corresponding to the Table S1, the vesicle morphology, and the osmolarity ratio P_e/P_0. The following rows contain the initial vesicle volume V_0, the initial area A_0, and the initial radius R_0 before the first deflation step, the apparent volume V_{app} and the apparent area A_{app} of the mother vesicle after the deflation step j, the total tube area $A = A_0 - A_{app}$, the total tube length L, and the fraction Λ of the total tube length corresponding to cylindrical tubes.

vesicle	Ld_1	Ld_2	Ld_3	Ld_4	Lo_1	Lo_2	Lo_3	Lo_4
lipid phase	Ld	Ld	Ld	Ld	Lo	Lo	Lo	Lo
defl. step j	1	2	3	4	1	2	3	4
morph.	VM-A	VM-B	VM-C	VM-C	VM-A	VM-B	VM-B	VM-C
P_e/P_0	1.25	1.38	1.51	1.64	1.25	1.38	1.51	1.64
V_0 [μm^3]	49296	30138	10223	30590	37384	14991	35177	37210
A_0 [μm^2]	6500	4683	2278	4730	5407	2940	5192	5390
R_0 [μm]	22.7	19.3	13.5	19.4	20.7	15.3	20.3	20.7
V_{app} [μm^3]	43997	25671	8350	24030	33378	12770	28730	29230
A_{app} [μm^2]	6027	4208	1992	4049	5053	2642	4536	4754
A [μm^2]	473	475	286	681	354	298	656	636
L [μm]	600	600	395	953	94	100	200	195
Λ	0	0	$\frac{1}{2} \pm \frac{1}{2}$ [a]	$\frac{1}{2} \pm \frac{1}{2}$ [a]	0	0	0	0.46

[a] For the VM-C morphology of the Ld membranes, we used the estimate $\Lambda = \frac{1}{2} \pm \frac{1}{2}$ corresponding to the whole range $0 \leq \Lambda \leq 1$ of possible Λ-values.

Table S3: **Overlap of PEG and dextran chains along the deflation path:** The osmotic deflation steps generate the compositions j with total polymer concentration c_j inside the vesicles, irrespective of whether the interior solution is uniform or phase separated. This concentration determines the reduced polymer concentration $\epsilon = |c_{cr} - c|/c_{cr}$ which measures the distance from the critical consolute point with concentration c_{cr}. For the PEG and dextran chains studied here, the radii of gyration have been estimated to be $R_p = 4.05\,\text{nm}$ and $R_d = 21\,\text{nm}$. [9] The overlap concentrations of PEG and dextran are then given by $1/[(4\pi/3)R_p^3] = 0.00359/\text{nm}^3$ and $1/[(4\pi/3)R_d^3] = 0.0258/(10\,\text{nm})^3$ which are equivalent to the overlap weight fractions $w_p^* = 0.0477$ and $w_d^* = 0.0193$. We characterize the degree of overlapping and the associated strength of repulsive chain-chain interactions by the overlap ratios w_p/w_p^* and w_d/w_d^*. Columns 4 and 5 display the overlap ratios of the PEG and dextran chains within the one-phase region. In this region, the large dextran chains overlapped already at the lowest dextran concentration while the smaller PEG chains did not overlap with each other but always overlapped with the dextran chains. The corresponding ratios after phase separation are shown in columns 6 and 7 for the PEG-rich phase as well as in columns 8 and 9 for the dextran-rich phase. In the PEG-rich phase, the overlap of the PEG chains increased with each deflation step whereas the dextran chains became separated after the third step. In the dextran-rich phase, the dextran chains overlapped more and more strongly whereas the PEG chains became more and more dilute but had to overlap with the dextran chains. Thus, all polymer solutions along the deflation path were semi-dilute.

comp. j	c_j [g/cm^3]	ϵ	$\dfrac{w_p}{w_p^*}$	$\dfrac{w_d}{w_d^*}$	$\dfrac{w_p^{PE}}{w_p^*}$	$\dfrac{w_d^{PE}}{w_d^*}$	$\dfrac{w_p^{DE}}{w_p^*}$	$\dfrac{w_d^{DE}}{w_d^*}$
0e	0.0664		0.69	1.69				
0	0.0714	0.139	0.65	2.02				
1	0.0800	0.035	0.73	2.26				
cr	0.0829	0	0.76	2.34				
2	0.0838	0.011			0.94	1.36	0.57	3.53
3	0.0875	0.055			1.09	0.79	0.46	4.42
4	0.0909	0.097			1.18	0.56	0.39	5.03
7	0.1002	0.209			1.38	0.25	0.28	6.78

Movie Ld_1: Morphology VM-A of Ld membrane

Giant vesicle bounded by an Ld membrane (red) after the first deflation step. The interior aqueous solution had total polymer mass density $c_1 = 1.120\,c_0 = 0.965\,c_{cr}$ and formed a uniform aqueous phase within the giant vesicle. The movie contains the 3-dimensional scan of the vesicle, provided by a stack of 44 confocal scans corresponding to different separations z from the cover slide, varying from $z = 1\,\mu$m to $z = 44\,\mu$m in increments of $1\,\mu$m. The scan reveals many nanotubes that protrude into the vesicle interior. The thickness of these tubes is below optical resolution; the total tube length is $600 \pm 100\,\mu$m.

Movie Ld_2: Morphology VM-B of Ld membrane

Giant vesicle with an Ld membrane (red) after the second deflation step. The interior aqueous solution had total polymer mass density $c_2 = 1.174\,c_0 = 1.024\,c_{cr}$ and was separated into two aqueous phases forming a PEG-rich and a dextran-rich droplet. The membrane was completely wetted by the PEG-rich phase and, thus, not in contact with the pd interface between the two aqueous droplets. The movie contains the 3-dimensional scan of the vesicle, provided by a stack of 37 confocal scans corresponding to different separations z from the cover slide, varying from $z = 1\,\mu$m to $z = 37\,\mu$m in increments of $1\,\mu$m. The Ld membrane has formed many nanotubes that protrude into the vesicle interior but are excluded from the dextran-rich phase which is in touch with the cover slide and thus located at low z-values. The thickness of these tubes is below optical resolution; the total tube length is $600 \pm 100\,\mu$m.

Movie Ld_4: Morphology VM-C of Ld membrane

Giant vesicle with an Ld membrane (red) after the fourth deflation step. The interior aqueous solution had total polymer mass density $c_4 = 1.273\,c_0 = 1.097\,c_{cr}$ and was phase separated into a PEG-rich and a dextran-rich droplet. The membrane was partially wetted by the PEG-rich phase and formed effective contact angles, θ_p and θ_d, with the pd interface between the two aqueous droplets (Fig. S3a). The movie contains the 3-dimensional scan of the vesicle, provided by a stack of 82 confocal scans corresponding to different separations z from the cover slide, varying from $z = 0.5\,\mu$m to $z = 41\,\mu$m in increments of $0.5\,\mu$m. The scan shows many nanotubes that protrude into the vesicle interior and aggregate at the pd interface because of partial wetting. The thickness of these tubes is below optical resolution; the total tube length is $953 \pm 150\,\mu$m.

Movie Lo_1: Morphology VM-A of Lo membrane

Giant vesicle with an Lo membrane (green) after the first deflation step. The interior aqueous solution had total polymer mass density $c_1 = 1.120\,c_0 = 0.965\,c_{\mathrm{cr}}$ and formed a uniform aqueous phase within the vesicle. The movie contains the 3-dimensional scan of the vesicle, provided by a stack of 74 confocal scans corresponding to different separations z from the cover slide, varying from $z = 0.5\,\mu$m to $z = 37\,\mu$m in increments of $0.5\,\mu$m. The Lo membrane has formed many nanotubes that protrude into the vesicle interior. The tube morphology can be optically resolved and is provided by short necklace-like tubes; the total tube length is $94 \pm 14\,\mu$m.

Movie Lo_2: Morphology VM-B for Lo membrane

Giant vesicle with an Lo membrane (green) after the second deflation step. The interior aqueous solution had total polymer mass density $c_2 = 1.174\,c_0 = 1.024\,c_{\mathrm{cr}}$ and was phase separated into a PEG-rich and a dextran-rich droplet. The membrane was completely wetted by the PEG-rich phase and, thus, not in contact with the pd interface between the two aqueous droplets. The movie contains the 3-dimensional scan of the vesicle, provided by a stack of 58 confocal scans corresponding to different separations z from the cover slide, varying from $z = 0.5\,\mu$m to $z = 29\,\mu$m in increments of $0.5\,\mu$m. The scan reveals many nanotubes protruding into the vesicle interior without entering the dextran-rich phase which is in touch with the cover slide and thus located at low z-values. The tube morphology can be optically resolved and is provided by necklace-like tubes with an average bead radius of $0.63\pm0.10\,\mu$m.

Movie Lo_4: Morphology VM-C for Lo membrane

Giant vesicle with an Lo membrane (green) after the fourth deflation step. The interior aqueous solution had total polymer mass density $c_4 = 1.273\,c_0 = 1.097\,c_{\mathrm{cr}}$ and was phase separated into a PEG-rich and a dextran-rich droplet. The membrane was partially wetted by the PEG-rich phase and formed effective contact angles, θ_{p} and θ_{d}, with the pd interface between the two aqueous droplets (Fig. S3a). The movie contains the 3-dimensional scan of the vesicle, provided by a stack of 74 confocal scans corresponding to different separations z from the cover slide, varying from $z = 0.5\,\mu$m to $z = 37\,\mu$m in increments of $0.5\,\mu$m. The Lo membrane has formed long nanotubes that protrude into the vesicle interior and tend to aggregate at the pd interface because of partial wetting. Detailed analysis of this scan (Fig. 6 in the main text) reveals the coexistence of necklace-like tubes with bead radius $R_{\mathrm{ss}} = 0.64\pm0.12\,\mu$m and cylindrical tubes with tube diameter $2R_{\mathrm{cy}} = 0.55\pm0.07\,\mu$m.

References

[1] Seifert, U., Berndl, K. & Lipowsky, R. Shape Transformations of Vesicles: Phase Diagram for Spontaneous Curvature and Bilayer Coupling Model. *Phys. Rev. A* **44**, 1182–1202 (1991).

[2] Lipowsky, R. Coupling of Bending and Stretching Deformations in Vesicle Membranes. *Adv. Colloid Interface Sci.* **208**, 14–24 (2014).

[3] Lipowsky, R. Spontaneous Tubulation of Membranes and Vesicles Reveals Membrane Tension Generated by Spontaneous Curvature. *Faraday Discuss.* **161**, 305–331 (2013).

[4] Doi, M. & Edwards, S. *The Theory of Polymer Dynamics* (Clarendon Press, Oxford, 1986).

[5] Kierfeld, J., Niamploy, O., Sa-yakanit, V. & Lipowsky, R. Stretching of Semi-flexible Polymers with Elastic Bonds. *Eur. Phys. J. E* **14**, 17–34 (2004).

[6] Helfrich, W. & Harbich, W. Adhesion and Cohesion of Tubular Vesicles. *Chemica Scripta* **25**, 32–36 (1985).

[7] Baroji, Y. F., Oddershede, L. B., Reihani, S. N. S. & Bendix, P. M. Fluorescent Quantification of Size and Lamellarity of Membrane Nanotubes. *Eur. Biophys. J.* **43**, 595–602 (2014).

[8] Kusumaatmaja, H., Li, Y., Dimova, R. & Lipowsky, R. Intrinsic Contact Angle of Aqueous Phases at Membranes and Vesicles. *Phys. Rev. Lett.* **103**, 238103 (2009).

[9] Liu, Y., Lipowsky, R. & Dimova, R. Concentration Dependence of the Interfacial Tension for Aqueous Two-Phase Polymer Solutions of Dextran and Polyethylene Glycol. *Langmuir* **28**, 3831–3839 (2012).